Acta Cryst. (1998). B**54**, 834–850

Carbides $Ln_{10}Ru_{10}C_{19}$ (Ln = Y, Gd–Lu): Crystal Structure of their Subcells and the Superstructures of $Er_{10}Ru_{10}C_{19}$

Rolf-Dieter Hoffmann and Wolfgang Jeitschko

Anorganisch-Chemisches Institut, Universität Münster, Wilhelm-Klemm-Strasse 8, D-48149 Münster, Germany

(*Received 25 September 1997; accepted 1 April 1998*)

Abstract

The nine new rare earth ruthenium carbides (10/10/19) were prepared by arc-melting of the elemental components and subsequent annealing at 1173 K. Guinier powder patterns show these compounds to crystallize with a very pronounced subcell, which was solved from the single-crystal X-ray diffractometer data of $Er_{10}Ru_{10}C_{19}$, erbium ruthenium carbide: *Amm*2, $Z = 1$, $R = 0.031$ for 1088 structure factors and 39 variable parameters. The single-crystal film data of $Er_{10}Ru_{10}C_{19}$ reveal several superstructures. Two of these were refined from the single-crystal diffractometer data of multiple domain crystals; one of these in the space group *Cm*, $Z = 2$, $R = 0.057$ for 4848 F values and 147 variables; the other in *Amm*2, $Z = 8$, $R = 0.078$ for 2352 F values and 171 variables. In all of these structures most of the C atoms are paired with C—C distances corresponding to double bonds. Together with the Ru atoms, these C atoms form two-dimensionally infinite layers, which are separated from each other by the Er atoms. In the third dimension the ruthenium–carbon layers are linked by single C atoms and carbon pairs. The subcell shows the superposition of these isolated and paired C atoms, whereas in the idealized superstructures these C atoms are fully ordered and their atomic environments reflect this order. $Lu_{10}Ru_{10}C_{19}$ is a metallic conductor and Pauli-paramagnetic. The carbides $Ln_{10}Ru_{10}C_{19}$, with Ln = Gd–Tm, show Curie–Weiss behaviour with magnetic moments corresponding to the free Ln^{3+} ions. The magnetic ordering temperatures are all below 35 K. Chemical bonding in these compounds can be rationalized on the basis of simple concepts assuming the octet and the 18-electron rules to be valid for the C and Ru atoms, respectively.

1. Introduction

Investigations of the ternary systems of the rare earth metals with ruthenium and carbon have resulted in the characterization of several ternary compounds. Holleck (1972, 1977) was the first to prepare the cubic perovskite carbides $CeRu_3C$ and $ScRu_3C$. The isotypic compounds $LnRu_3C$ (Ln = Dy–Lu; Wachtmann *et al.*, 1995) were reported more recently. In these carbides the C atoms are isolated from each other and occupy octahedral voids formed by the ruthenium atoms. Sc_3RuC_4 also has a relatively simple structure, where the C atoms are paired (Hoffmann *et al.*, 1992). The carbides $Ln_7Ru_2C_{11}$ (Ln = Dy–Tm) crystallize with a complex superstructure, which contains isolated C atoms as well as C_2 pairs (Musanke, Jeitschko & Hoffmann, 1993). The structure of $Gd_{12}Ru_{7.5}C_{20}$ also has isolated C atoms and C_2 pairs. It shows considerable disorder resulting from the disordered arrangement of Ru atoms on a sixfold axis (Hoffmann & Jeitschko, 1990). Recently we reported the crystal structure of $GdRuC_2$ (Hoffmann *et al.*, 1995), where all C atoms are paired. This compound is stable only at very high temperature and can be obtained at room temperature only by very rapid quenching. In samples cooled at lower rates, the carbides of the present communication are obtained. Their composition, determined for $Er_{10}Ru_{10}C_{19}$ by crystal structure analyses, is very similar to that of $GdRuC_2$. Nevertheless, their (subcell) structure is quite different from that of $GdRuC_2$, even though most of the C atoms of the 10:10:19 compounds are also paired. Only 1/19 of these C atoms are unpaired. The complicated superstructures of the 10:10:19 carbides arise from the various ways the paired and unpaired C atoms are ordered in trigonal prisms formed by the Ru atoms. A preliminary account of the work reported here has been presented at a conference (Hoffmann & Jeitschko, 1987).

2. Sample preparation

Starting materials were filings of the rare earth metals, ruthenium powder (all with nominal purities > 99.9%) and graphite flakes (> 99.5%). Cold-pressed pellets (0.2–0.5 g) of the elemental components were reacted in an arc-melting furnace under an argon atmosphere, which was further purified by repeatedly melting a titanium button prior to the reactions. The buttons were remelted several times, turned around and remelted again to ensure good homogeneity. Material losses were of the order 2–3%, except for $Yb_{10}Ru_{10}C_{19}$, where they were caused by the low boiling point of ytterbium. The compounds were already present in the as-cast samples. Nevertheless, the compact samples were wrapped in

ISSN 0108-7681 © 1998

Table 1. *Lattice constants of the orthorhombic subcell of the ternary carbides $Ln_{10}Ru_{10}C_{19}$ (Ln = Y, Gd–Lu), as obtained from powder data of samples annealed at 1173 K*

Compound	*a* (Å)	*b* (Å)	*c* (Å)	*V* (Å^3)
$Y_{10}Ru_{10}C_{19}$	3.6526 (4)	18.697 (1)	7.3010 (6)	498.6 (1)
$Gd_{10}Ru_{10}C_{19}$	3.740 (4)	18.684 (4)	7.302 (2)	510.2 (7)
$Tb_{10}Ru_{10}C_{19}$	3.717 (6)	18.701 (6)	7.297 (6)	507.3 (1)
$Dy_{10}Ru_{10}C_{19}$	3.668 (2)	18.685 (2)	7.292 (1)	499.8 (4)
$Ho_{10}Ru_{10}C_{19}$	3.6292 (9)	18.639 (3)	7.285 (2)	492.8 (2)
$Er_{10}Ru_{10}C_{19}$	3.6059 (6)	18.632 (2)	7.2861 (6)	489.5 (1)
$Tm_{10}Ru_{10}C_{19}$	3.5849 (4)	18.586 (2)	7.2807 (7)	485.1 (1)
$Yb_{10}Ru_{10}C_{19}$	3.579 (1)	18.516 (9)	7.284 (3)	482.7 (3)
$Lu_{10}Ru_{10}C_{19}$	3.548 (2)	18.546 (8)	7.270 (4)	478.4 (3)

tantalum foil, sealed in evacuated silica tubes and annealed for 10 d at 1173 K to enhance their homogeneity. They were then quenched in ice–water. The samples were single-phase with the exception of the ytterbium-containing samples, for which $YbRu_3C$ was found to be a major impurity.

Single crystals of $Er_{10}Ru_{10}C_{19}$ were obtained by annealing arc-melted samples in a water-cooled silica tube in a high-frequency furnace slightly below the melting point for 10–30 min. Samples crystallized much better with a carbon content (Er:Ru:C = 10:10:17) smaller than that required by the composition of the ternary carbide (Er:Ru:C = 10:10:19).

The products were characterized by metallography and scanning electron microscopy. Energy-dispersive X-ray fluorescence analyses did not reveal any impurity elements heavier than sodium.

3. Lattice constants

Lattice constants of the subcell were obtained from Guinier powder patterns (Cu $K\alpha_1$) using α-quartz (a = 4.9130 and c = 5.4046 Å) as an internal standard. Indices could be assigned on the basis of the orthorhombic

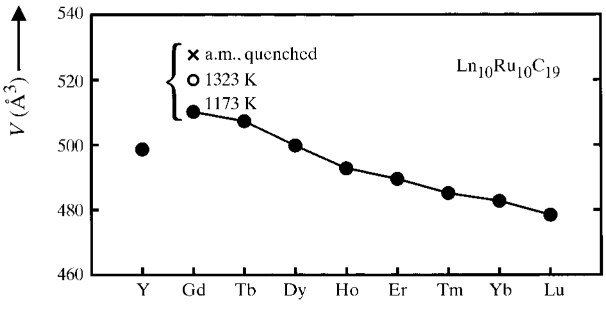

Fig. 1. Cell volumes of the subcell for the rare earth ruthenium carbides $Ln_{10}Ru_{10}C_{19}$. Filled circles indicate the cell volumes for samples with the ideal composition annealed at 1173 K. For the Gd compound larger lattice constants were obtained from samples with possibly slightly different compositions, which had been quenched after the arc-melting (a.m.) or after annealing at a higher temperature.

subcell found by the single-crystal investigations of $Er_{10}Ru_{10}C_{19}$. The identification of the diffraction lines was facilitated by intensity calculations (Yvon *et al.*, 1977) using the positional parameters of the structure determination. The lattice constants (Table 1) were obtained by least-squares fits.

A plot of the cell volumes shows the expected lanthanoid contraction (Fig. 1). It can be seen that the volume for the gadolinium compound deviates from the extrapolated value. Since the corresponding compounds with the earlier lanthanoids could not be prepared, we ascribe this behaviour to a deviation from the ideal composition of that sample, which was annealed, as were the others, at 1173 K. In samples of $Gd_{10}Ru_{10}C_{19}$, which had been quenched from higher temperatures, cell volumes as large as 527.7 (1) Å^3 [a = 3.8924 (2), b = 18.619 (1), c = 7.2808 (3) Å] were observed. It is well known that homogeneity ranges are larger at higher temperature. This was not investigated any further.

Lattice constants for the various crystals of the composition $Er_{10}Ru_{10}C_{19}$ were also obtained on a four-circle diffractometer. They were all in good agreement (the largest deviation was five standard deviations) with the corresponding ones calculated from the subcell reflections. Since the four-circle diffractometer intensities are all shifted to higher diffraction angles (due to absorption), they are all slightly too small. Therefore, the lattice constants derived from the Guinier powder pattern of the $Er_{10}Ru_{10}C_{19}$ samples quenched from high temperature were used in all cases for the calculation of the bond distances.

4. Chemical and physical properties

Well crystallized samples of the ternary carbides are grey with metallic lustre. They do not show any kind of deterioration in air over a period of several years. However, they react with hydrochloric acid, especially at higher temperature. The gaseous reaction products were analysed as reported earlier (Jeitschko *et al.*, 1989). Besides the expected gases CH_4, C_2H_4 and C_2H_6, also between 20 and 60 wt% C_3, C_4, C_5 and C_6 hydrocarbons were observed. Such higher hydrocarbons were also found as reaction products of other ternary and quaternary rare earth carbides, *e.g.* in samples of $SmRhC_2$ (Hoffmann *et al.*, 1989) and $ErFe_2SiC$ (Witte & Jeitschko, 1994), which contain only C_2 pairs or isolated C atoms, respectively.

Electrical conductivity measurements of an arc-melted ingot of $Lu_{10}Ru_{10}C_{19}$ reveal metallic behaviour. The electrical resistivity increases by a factor of eight between 5 and 300 K. At room temperature a resistivity of 50 μΩ cm was observed. Owing to the difficulty in estimating the sizes of the contacting areas, this value may be in error by a factor of up to two. Samples of $Y_{10}Ru_{10}C_{19}$ and $Lu_{10}Ru_{10}C_{19}$ were tested for superconductivity with an *ac* susceptometer. No superconducting transition was found for either compound down to 2 K.

The magnetic properties of the carbides $Ln_{10}Ru_{10}C_{19}$ (Ln = Gd–Tm) were investigated with a SQUID magnetometer at temperatures between 4 and 300 K, with magnetic flux densities up to 5.5 T. $Lu_{10}Ru_{10}C_{19}$ is Pauli-paramagnetic, indicating that the ruthenium–carbon polyanion does not carry localized magnetic moments. The other carbides show Curie–Weiss behaviour with magnetic ordering temperatures all lower than 35 K. The magnetic moments calculated from the slopes of the linear portions of the $1/\chi$ *versus* T plots are all in good agreement with the magnetic moments expected for the free Ln^{3+} ions.

5. Structure determinations

Single crystals of $Er_{10}Ru_{10}C_{19}$ were investigated with Weissenberg and Buerger precession cameras. Reciprocal layer photographs of four crystals were taken. While the reciprocal lattices of the four crystals did not show any differences for the basic (subcell) structure, different types of superstructure reflections were

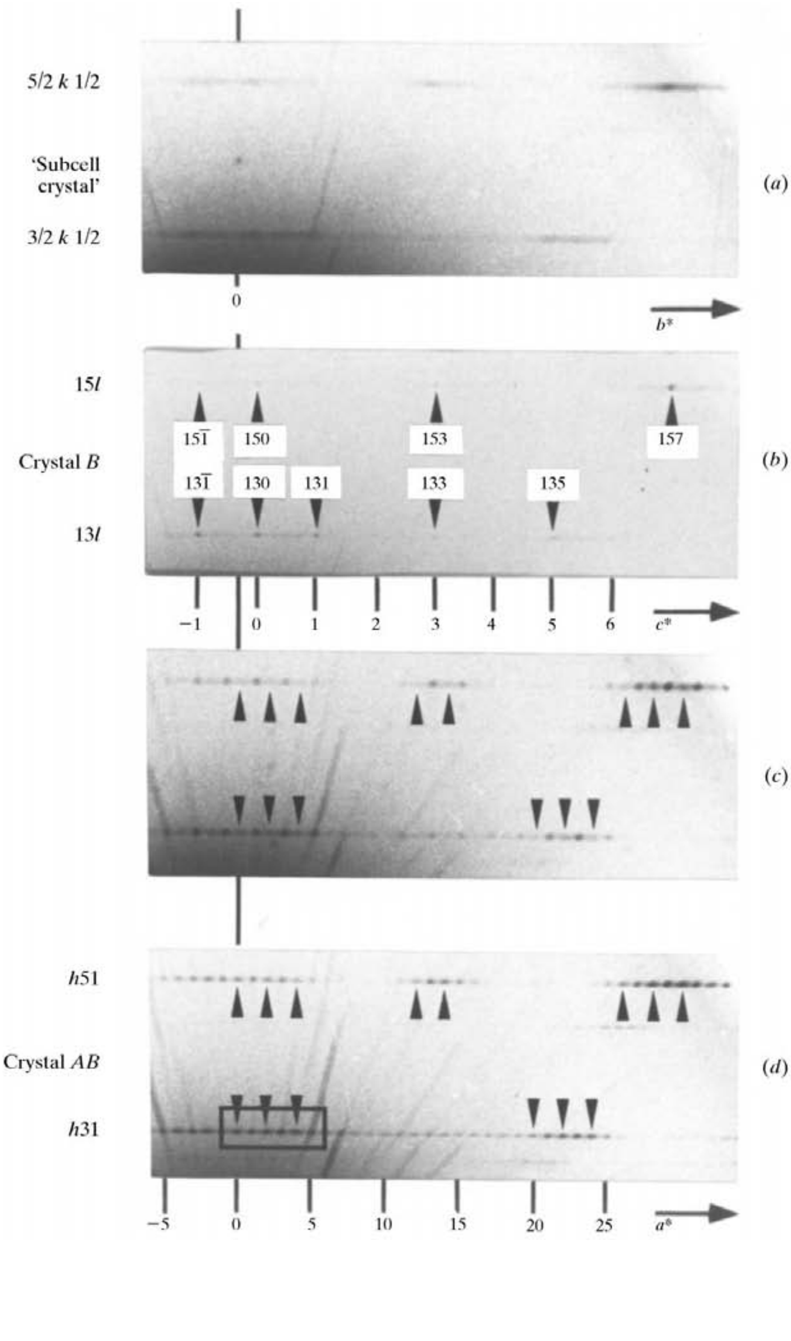

Fig. 2. Two reciprocal lattice rows of superstructure reflections as recorded from four different crystals in a precession camera using unfiltered Mo $K\alpha$ radiation. The top of the figure (*a*) shows an overexposed photograph of the two reciprocal lattice rows $\frac{3}{2},k,\frac{1}{2}$ and $\frac{5}{2},k,\frac{1}{2}$ of the crystal used for the structure refinement of the subcell. These diffuse superstructure rows were (by definition) neglected when the subcell data were recorded. The second and fourth photographs, (*b*) and (*d*), show the corresponding reciprocal lattice rows of the crystals *B*-$Er_{10}Ru_{10}C_{19}$ and *AB*-$Er_{10}Ru_{10}C_{19}$. Note the reflections marked with arrows in the third and fourth photographs, (*c*) and (*d*). These reciprocal lattice points cannot be rationalized as due to twinning of the *B* structure, since they do not occur in the monoclinic reciprocal lattice of crystal *B*. No subcell reflections are shown on these four photographs; they are approximately ten times as strong as the superstructure reflections. The enframed reciprocal lattice reflections of crystal *AB* (*d*) are further discussed in the text.

Table 2. *Crystal data of the subcell crystal and crystals B and AB of $Er_{10}Ru_{10}C_{19}$*

Chemical formula	$Er_{10}Ru_{10}C_{19}$ (subcell)	$Er_{10}Ru_{10}C_{19}$ (*B*)	$Er_{10}Ru_{10}C_{19}$ (*AB*)
Space group	*Amm*2 (No. 38)	*Cm* (No. 8)	*Amm*2 (No. 38)
a (Å)†	3.6097 (4)	14.578 (2)	37.264 (4)
b (Å)†	18.632 (2)	7.219 (1)	7.219 (2)
c (Å)†	7.289 (1)	10.004 (2)	14.578 (2)
β (°)†		111.36 (5)	
V (Å^3)	490.2	980.5	3921.6
Z	1	2	8
Chemical formula weight	2911.5	2911.5	2911.5
D_x (g cm^{-3})	9.86	9.86	9.86
Dimensions (µm^3)	9 × 17 × 55	11 × 22 × 24	25 × 25 × 65
Radiation	Mo $K\alpha$	Mo $K\alpha$	Mo $K\alpha$
μ (mm^{-1})	49.7	49.7	49.7
$2\theta_{max}$ (°)	70	80	50
hkl range	$-5 \rightarrow h \rightarrow 5$	$-26 \rightarrow h \rightarrow 26$	$-44 \rightarrow h \rightarrow 44$
	$-30 \rightarrow k \rightarrow 30$	$0 \rightarrow k \rightarrow 13$	$-8 \rightarrow k \rightarrow 8$
	$-11 \rightarrow l \rightarrow 11$	$-18 \rightarrow l \rightarrow 18$	$-17 \rightarrow l \rightarrow 17$
Total number of reflections	4282	6588	13 797
Absorption correction	From ψ scans	None	From ψ scans
Transmission ratio (max./min.)	1.21	1.64	1.33
Unique reflections	1239	6588	3814
Internal residual	0.069	—	0.038
Reflections with $I > n\sigma(I)$	1088 (n = 2)	4848 (n = 3)	2352 (n = 2)
Number of variables‡	44/39	147	171
Residual (subcell F values)‡	0.050/0.031 (1088)	0.049 (3150)	0.019 (526)
Residual (superstructure F values)	—	0.092 (1698)	0.182 (1826)
Residual (subcell + superstructure)	—	0.057 (4848)	0.078 (2352)
Residual (all F values)‡	0.065/0.042 (1239)	0.084 (6588)	0.127 (3814)
Weighted residual (all I values)‡	0.133/0.063 (1239)	0.162 (6588)	0.032 (3814)
Weighting parameter *a*/*b*	0.0083/26	0.089/83	0/0

† Calculated from powder data of a sample quenched from above 1473 K. ‡ The first values for the refinement of the subcell data correspond to the upper part of Table 3, the second values correspond to the refinement shown in the lower part of Table 3.

observed, suggesting a variety of superstructures and twinning (Fig. 2).

Intensity data were collected for three single crystals. One crystal showed sharp (basic) subcell reflections, while the superstructure reflections were visible as diffuse streaks extending along one reciprocal lattice direction, the b^* direction (Fig. 2*a*). Reciprocal lattice planes were also recorded perpendicular to this direction, confirming the strictly one-dimensional character of these diffuse streaks and, consequently, the disorder of the structure is confined to one dimension. This crystal (with the space-group symmetry *Amm*2) will be termed the *subcell crystal* throughout the paper. The corresponding crystal structure is termed the *subcell structure*. However, one should keep in mind that this subcell is the same for all crystals. Another crystal (Fig. 2*b*) showed well developed superstructure reflections with the symmetry *Cm*. From the data collected for this crystal we refined a superstructure, which we designated with the letter *B*, and, consequently, we term this crystal *crystal B*. The third crystal also showed well developed superstructure reflections. The symmetry is *Amm*2, the same as for the subcell but with an eightfold larger cell volume. For this crystal we determined a structure, which we term the *AB structure*, and, therefore, we refer to this crystal as *crystal AB*. Details of the data collections are given in Table 2. The relationships of the various lattices are illustrated in Fig. 3.

The structures were refined, minimizing $wR_2 = [\Sigma w(F_o^2 - F_c^2)^2/\Sigma w(F_o^2)^2]^{1/2}$, by the full-matrix least-squares program *SHELXL*93 (Sheldrick, 1993) with atomic scattering factors, corrected for anomalous dispersion (*International Tables for Crystallography*, 1992), as provided by this program. The weighting scheme was based on the counting statistics with $w = 1/[\sigma^2 + aP + (bP)^2]$, where σ is the standard deviation of the observed intensity, and a and b were chosen such as to obtain a flat regression of variance in terms of the magnitude of I_c and $P = [\max(I_o, 0) + 2(I_c)/3]$. A factor e, correcting for secondary extinction, was refined and applied to the calculated structure factors as given by $[1 + 0.001eI_c\lambda^3/\sin 2\theta]^{-1/4}$. Since all structures of $Er_{10}Ru_{10}C_{19}$ crystallize in non-centrosymmetric space groups, polar axis restraints were applied by the method of Flack & Schwarzenbach (1988) and the absolute structures of the crystals were established, as described by Flack (1983).

5.1. *Subcell structure*

The crystal of Fig. 2(*a*) showed only diffuse superstructure reflections extending along one well defined reciprocal lattice direction. Therefore, the sharp subcell reflections were judged to correspond best to the average structure. The subcell reflections showed orthorhombic symmetry with the extinction condition of an A-centred lattice. Of the three possible space groups *Ammm*, *Amm*2 and *A*222, the non-centrosymmetric group *Amm*2 was found to be correct in the course of the structure determination.

The erbium positions were found by interpretation of the Patterson function; the other atoms were located by subsequent difference Fourier syntheses. The results of two different 'final' refinements of the subcell data are shown in Table 3. In the upper part of Table 3, the atomic positions as obtained with anisotropic displacement parameters for the metal atoms and the C5 position are listed. With the exception of the four carbon positions C1–C4, all atoms had (mostly) cigar-shaped displacement parameters. Therefore, we also refined the subcell data, where all these atoms were allowed to occupy split positions. These refinements were carried out with isotropic displacement parameters, and the results are listed in the lower part of Table 3. A drawing with the atomic positions of this refinement is presented in Fig. 4. In this drawing the splitting of the Ru and C5 positions is not visible, because it occurs along the viewing direction. The near-neighbour environments as obtained from the refinement with anisotropic displacement parameters are shown in Fig. 5 and the interatomic distances of this refinement are listed in Table 4. The residuals of the refinements of the subcell with anisotropic displacement parameters and with isotropic displacement parameters, but with split positions, are listed in Table 2. The subcell was also refined from the subcell data of the crystals B and AB. These results were quite similar to those presented in Table 3 and, therefore, these data as well as the data for the AB structure

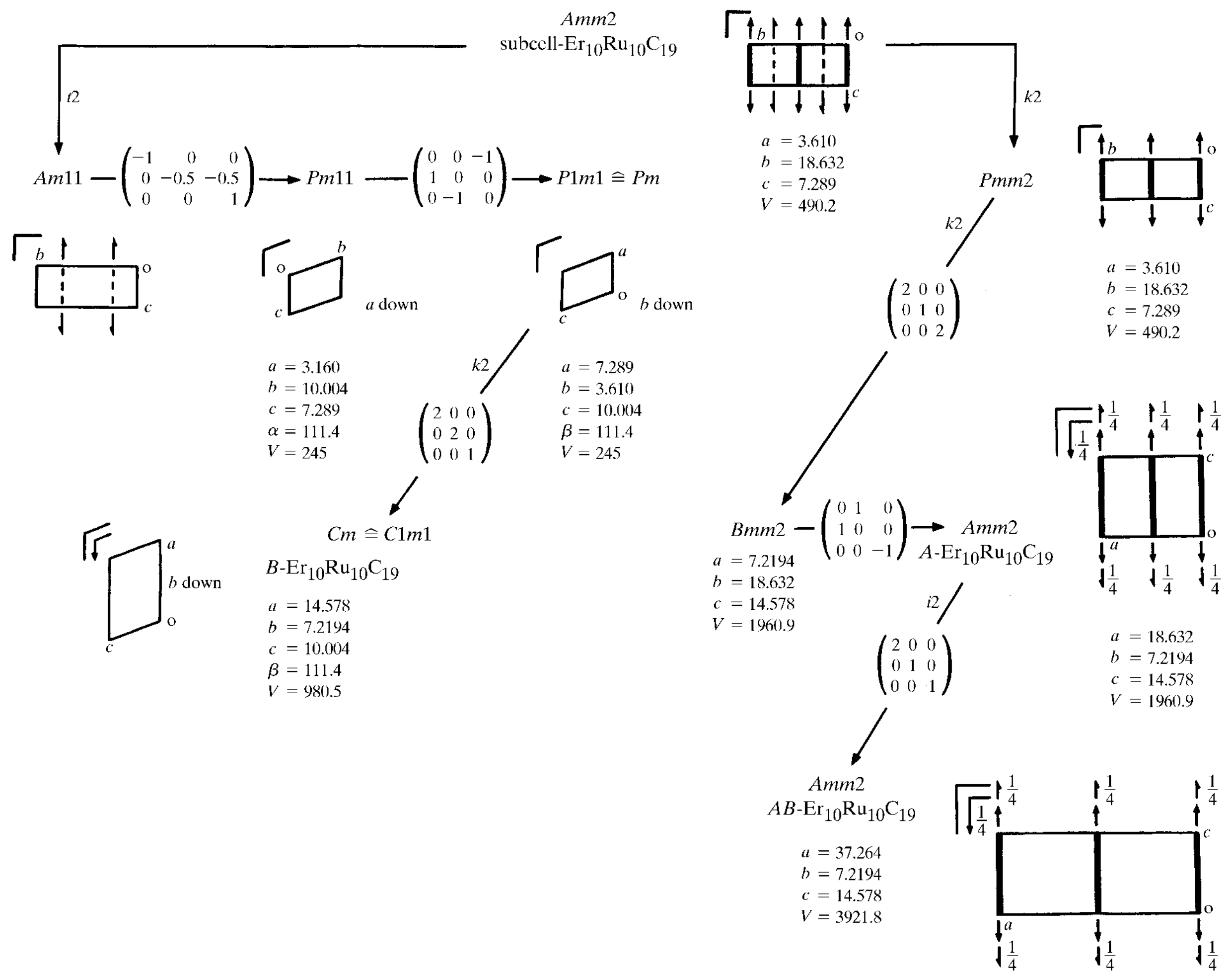

Fig. 3. Space-group relationships of various structures of $Er_{10}Ru_{10}C_{19}$. The space group *Amm*2 of the subcell is shown at the top. Going from top to bottom the symmetry is lowered in single steps by either a *translationengleiche* (t), a *klassengleiche* (k) or the special *klassengleiche*, the isomorphic (i) reduction (*International Tables for Crystallography*, 1983). The transformation matrices, lattice constants together with unit-cell volumes and indices t, k and i for the subgroups are also given. Horizontal arrows indicate cell transformations between equivalent settings.

Table 3. *Atomic parameters of the subcell of $Er_{10}Ru_{10}C_{19}$*

Refinement with anisotropic displacement parameters for the metal atoms and C5.

	*Amm*2	Occupancy	*x*	*y*	*z*	B_{eq}
Er1	4(*d*)	1	0.0	0.1194 (1)	0.6131 (2)	0.92 (3)
Er2	4(*d*)	1	0.0	0.19151 (8)	0.1624 (2)	0.46 (2)
Er3	2(*a*)	1	0.0	0.0	0.0198 (5)	1.19 (4)
Ru1	4(*e*)	1	1/2	0.0730 (2)	0.3050 (5)	2.66 (9)
Ru2	4(*e*)	1	1/2	0.2035 (1)	0.8495 (4)	0.49 (4)
Ru3	2(*b*)	1	1/2	0.0	0.6439 (6)	2.1 (1)
C1	4(*e*)	1	1/2	0.0848 (9)	0.855 (3)	0.2 (2)†
C2	4(*e*)	1	1/2	0.102 (2)	0.037 (4)	0.2†
C3	4(*e*)	1	1/2	0.176 (1)	0.409 (3)	0.2†
C4	4(*e*)	1	1/2	0.219 (2)	0.563 (3)	0.2†
C5	4(*c*)	3/4	0.110 (1)	0.0	0.380 (1)	1.0‡

Refinement with isotropic displacement parameters and split positions for most atoms.

	*Amm*2	Occupancy	*x*	*y*	*z*	B_{iso}
Er1*a*	4(*d*)	1/2	0.0	0.11293 (8)	0.6039 (2)	0.32 (1)†
Er1*b*	4(*d*)	1/2	0.0	0.12562 (8)	0.6261 (2)	0.32†
Er2*a*	4(*d*)	1/2	0.0	0.1944 (1)	0.1634 (5)	0.41 (1)†
Er2*b*	4(*d*)	1/2	0.0	0.1885 (2)	0.1650 (6)	0.41†
Er3*a*	2(*a*)	1/2	0.0	0.0	0.0442 (3)	0.37 (2)†
Er3*b*	2(*a*)	1/2	0.0	0.0	0.9997 (3)	0.37†
Ru1	8(*f*)	1/2	0.4251 (4)	0.07306 (7)	0.3073 (2)	0.24 (2)
Ru2	8(*f*)	1/2	0.480 (1)	0.20337 (6)	0.8515 (2)	0.35 (2)
Ru3	4(*c*)	1/2	0.4321 (5)	0.0	0.6460 (3)	0.24 (3)
C1	4(*e*)	1	1/2	0.0813 (6)	0.850 (2)	0.1 (1)†
C2	4(*e*)	1	1/2	0.1026 (7)	0.031 (2)	0.1†
C3	4(*e*)	1	1/2	0.1777 (8)	0.407 (2)	0.5 (1)†
C4	4(*e*)	1	1/2	0.2167 (8)	0.567 (2)	0.5†
C5*a*	4(*c*)	1/2	0.210 (8)	0.0	0.423 (4)	0.4‡
C5*b*	2(*a*)	1/2	0.0	0.0	0.427 (5)	0.4‡

† These displacement parameters were refined constrained. ‡ These parameters were not refined.

and the proposed *A* structure (see below) are only deposited.†

5.2. *The superstructure B-$Er_{10}Ru_{10}C_{19}$*

The superstructure reflections of crystal *B* (Fig. 2*b*) required a doubling of both the *a* and *c* translation periods of the subcell. The structure was eventually refined in the space group *Cm*. The space-group relationships are outlined in Fig. 3. It can be seen that the symmetry is lowered from the subcell to the superstructure *B* in two steps. Rotational symmetry is lost by the *translationengleiche* transformation from *Amm*2 to *Am*11. This latter group is a non-standard setting of the space group *Pm*. In a second step, represented by a (minimal) *klassengleiche* transformation, two translation lengths of the subcell are doubled, resulting in a centred lattice of the space group *Cm*.

The monoclinic *Cm* symmetry of the crystal *B* was clearly visible on the precession diagrams. However, because of the loss of the rotational symmetry (transformation *Amm*2 → *Am*11, Fig. 3) twinning could be expected (Wondratschek & Jeitschko, 1976) and indeed was observed. The intensity data of both twin domains were recorded simultaneously on the four-circle diffractometer by assuming the common pseudo-orthorhombic *F*-centred cell (a = 37.264, b = 7.219, c = 14.578 Å; the transformation matrices from this cell to the cells of the two twin domains are $0,0,1/0,1,0/-\frac{1}{4},0,-\frac{1}{4}$ for the large twin domain, and $0,0,1/0,1,0/+\frac{1}{4},0,-\frac{1}{4}$ for the small twin domain). Eventually the structure could be refined for both twin domains independently.

A model for the superstructure was readily visualized by considering the true cell dimensions and the split atomic positions, as shown on the left-hand side of Fig. 6(*a*). The most significant splitting occurs for the C5 position. 33.3% of the C5 atoms (C5*b* atoms) are situated on the mirror plane, which extends perpendicular to the x_{sub} direction. The other C5 atoms (C5*a* atoms) are situated to the left and right of that mirror plane with a C5*a*—C5*a* bond distance of 1.4 Å. Thus, 33.3% of the C5 atoms are single C atoms (C5*b* atoms) and the other 66.7% form $(C5a)_2$ pairs. It was assumed that the split positions of the Er1, Er3, Ru1 and Ru3 atoms reflect the arrangement of the C5 atoms. The trigonal prism formed by the Ru atoms should be elongated or compressed, depending on whether it contains a $(C5a)_2$ pair or a

† Supplementary data for this paper are available from the IUCr electronic archives (Reference: SH0107). Services for accessing these data are described at the back of the journal.

single C5*b* atom. Since superstructure *B* requires a doubling of both the *a* and *c* dimensions of the subcell, it was assumed that these doublings were due to the alternating arrangement of elongated and compressed ruthenium prisms containing the $(C5a)_2$ pairs and the single C5*b* atoms, respectively. With this model for the *B* superstructure the corresponding data were refined successfully. In order to account for the twinning, the scale factors for the (common) subcell (of both twin orientations) and the superstructure reflections had to be varied independently. It turned out that the superstructure reflections of the larger twin domain accounted for 29.2 (3)% of the total volume (as scaled from the subcell data) and 10.6 (2)% corresponded to the volume of the other twin domain. Thus, together the superstructure reflections of both twin domains only accounted for 39.8% of the total volume of the twinned crystal. For the remaining 60.2% of the total volume no long-range order (as manifested by the superstructure reflections) was observed. The corresponding superstructure intensities were too diffuse to be recorded. The results are listed in Tables 2, 5 and 6. The atom labels as used for the refinement of the subcell data with split atomic positions (lower part of Table 3) were retained for the refinement of the superstructure (Table 5). This means that an Er1*a* atom of the subcell also remained an Er1*a* atom in the superstructure; however, since the asymmetric unit is twice as large in the superstructure, there are also two positions for the Er1*a* atom in the superstructure which were designated by the labels Er1*aα* and Er1*aβ*. No distinctions by Greek letters were needed for the Er3, Ru3 and the C5 atoms. For these atoms the lowering of the symmetry in the superstructure did not result in additional atomic positions.

5.3. *Crystal AB*

Intensity data were also recorded for a third crystal, which we designated using the label *AB*. The reciprocal lattice of this crystal clearly shows orthorhombic symmetry with the lattice constants a = 37.264 (4), b = 7.219 (2), c = 14.578 (2) Å. The systematic extinctions correspond to the large *A*-centred cell shown at the bottom of Fig. 3. This cell cannot be interpreted as due to twinning of a crystal with the monoclinic superstructure *B*, as demonstrated in Fig. 7(*b*). Therefore, we first determined and successfully refined a structure for this large *A*-centred cell, which we term the *AB* structure. This structure is composed of four building blocks in the stacking sequence *ABAB*, *ABAB*, as shown in Fig. 8. The refinement resulted in an overall conventional residual (on *F* values) of R = 0.101 for 2352 *F* values and 132 variable parameters (wR_2 = 0.0526). For the 1826 superstructure reflections (Hoffmann, 1996) the residual amounted to R = 0.214. The difference Fourier synthesis showed residual electron densities at positions which differed from the occupied positions by $\Delta y = \frac{1}{2}$. These residual positions correspond to a struc-

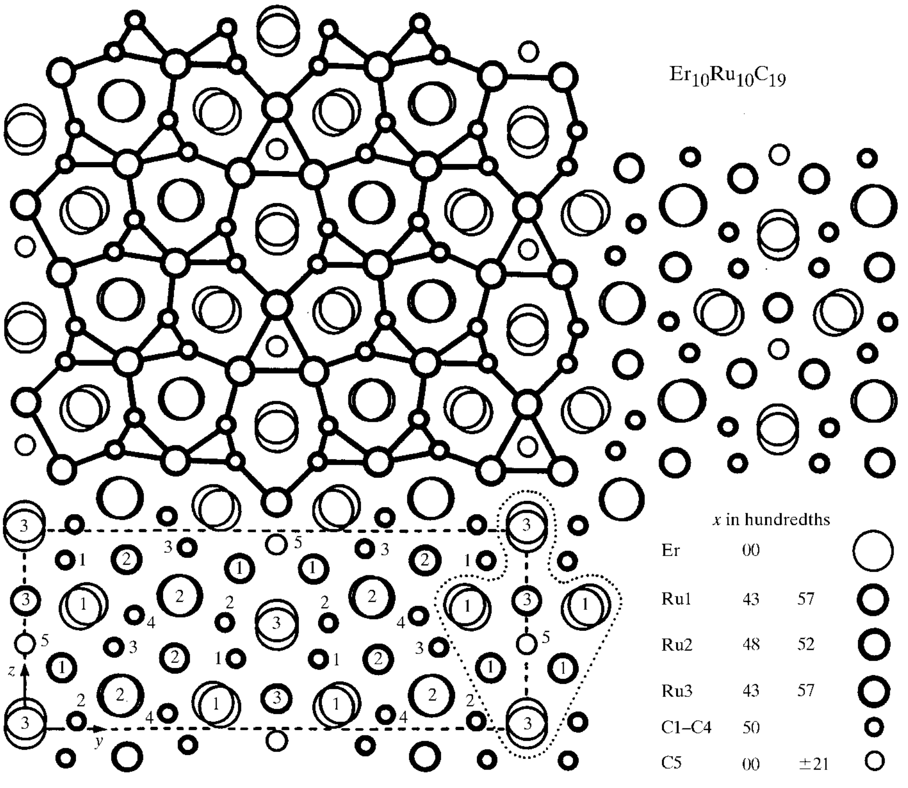

Fig. 4. The structure of the orthorhombic (*Amm*2) subcell of $Er_{10}Ru_{10}C_{19}$. In the upper part of the drawing the ruthenium–carbon polyanion (situated on the mirror plane at x = 0.5) is emphasized. The C atoms of this polyanion are positioned exactly on the mirror plane, while the Ru atoms are in split positions above and below the mirror plane. The Er atoms (where the single-digit numbers indicate the atom designations) are all situated on the mirror plane at x = 0; they occupy split positions within the plane. The C5 atoms occupy split positions, which are all superimposed when viewed along the projection direction. The various superstructures are caused by the ordered distributions of the C5 atoms. The atoms within the dotted line are shown in the projection along the y direction on the left-hand side of Fig. 6(*a*).

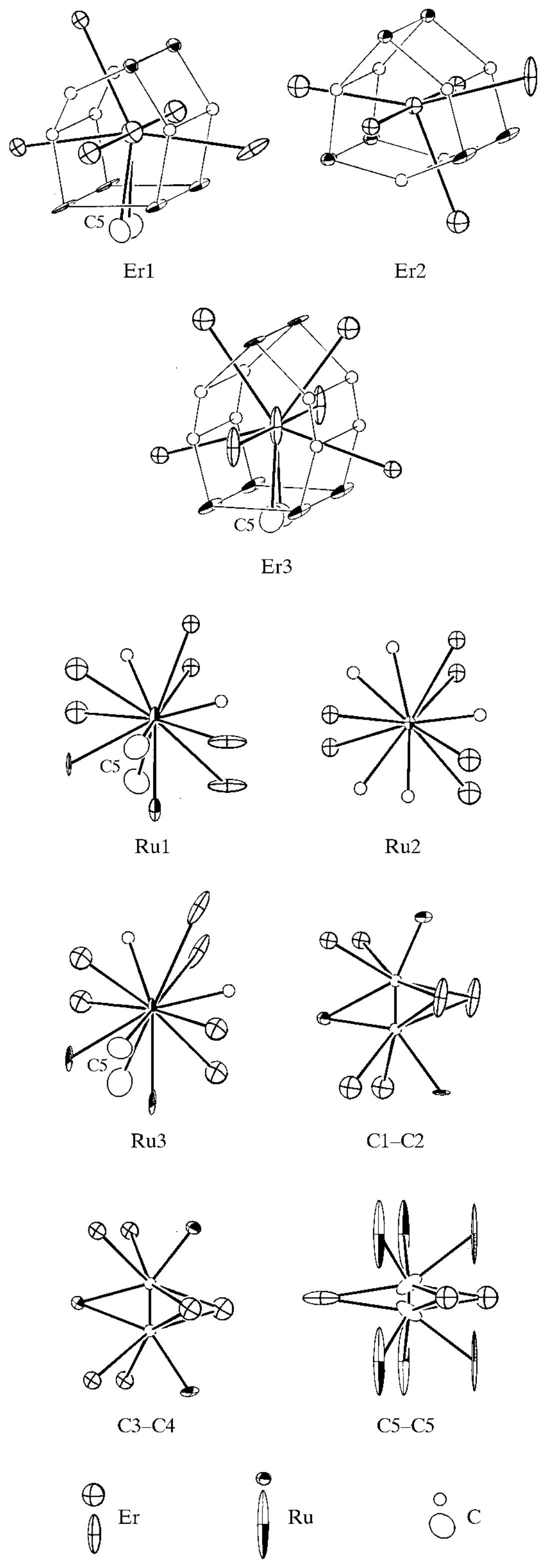

Fig. 5. Near-neighbour environments of all atoms in the subcell corresponding to the positional parameters as listed in the upper part of Table 3. The anisotropic displacement parameters are drawn at the 95% probability limit.

Table 4. *Interatomic distances in the subcell of* $Er_{10}Ru_{10}C_{19}$

The distances were calculated with the atomic positions as obtained in the refinement with anisotropic displacement parameters (upper part of Table 3). The standard deviations are all equal to or less than 0.001 (Er—Er, Er—Ru, Ru—Ru), 0.02 (Er—C, Ru—C) and 0.04 Å (C—C). All distances shorter than 4.2 (Er—Er, Er—Ru), 3.9 (Er—C, Ru—Ru) and 2.9 Å (Ru—C, C—C) are listed. Interatomic distances listed in parentheses do not occur in the real (super)structures.

Er1—2C3	2.57	Ru2—1C1	2.21
Er1—2C1	2.60	Ru2—1C3	2.28
Er1—2C4	2.61	Ru2—1C2	2.33
Er1—1.5C5	2.83	Ru2—2Ru2	3.610
Er1—2Ru3	2.873	Ru2—2Er2	2.917
Er1—2Ru2	2.945	Ru2—2Er1	2.946
Er1—2Ru1	3.008	Ru2—2Er2	2.991
Er1—1Er2	3.542	Ru3—2C1	2.20
Er1—1Er2	3.558	Ru3—1.5C5	2.38
Er1—2Er1	3.610	(Ru3—1.5C5	2.92)
Er1—1Er3	3.705	Ru3—2Ru1	2.819
Er2—2C4	2.56	Ru3—2Ru3	3.610
Er2—2C3	2.56	Ru3—4Er1	2.873
Er2—2C2	2.63	Ru3—2Er3	3.281
Er2—2Ru2	2.917	C1—1C2	1.36
Er2—2Ru2	2.991	C1—1Ru3	2.20
Er2—2Ru1	3.036	C1—1Ru2	2.21
Er2—1Er1	3.542	C1—2Er1	2.60
Er2—1Er1	3.550	C1—2Er3	2.68
Er2—2Er2	3.610	C2—1C1	1.36
Er2—1Er3	3.716	C2—1Ru1	2.03
Er3—4C2	2.62	C2—1Ru2	2.33
Er3—1.5C5	2.66	C2—2Er3	2.62
Er3—4C1	2.68	C2—2Er2	2.63
Er3—4Ru1	3.071	C3—1C4	1.38
Er3—2Ru3	3.281	C3—1Ru1	2.07
Er3—2Er3	3.610	C3—1Ru2	2.28
Er3—2Er1	3.705	C3—2Er2	2.56
Er3—2Er2	3.716	C3—2Er1	2.57
Ru1—1C2	2.03	C4—1C3	1.38
Ru1—1.5C5	2.03	C4—1Ru2	2.11
Ru1—1C3	2.07	C4—1Ru2	2.13
Ru1—1.5C5	2.65	C4—2Er2	2.56
Ru1—1Ru1	2.720	C4—2Er1	2.61
Ru1—1Ru3	2.819	(C5—C5	0.80)
Ru1—2Ru1	3.610	C5—2Ru1	2.03
Ru1—2Er1	3.008	C5—1Ru3	2.38
Ru1—2Er2	3.036	C5—2Ru1	2.65
Ru1—2Er3	3.071	(C5—1Ru3	2.92)
Ru2—1C4	2.11	C5—1Er3	2.66
Ru2—1C4	2.13	C5—2Er1	2.83

ture $A'B'A'B'$, $A'B'A'B'$, where the open and closed triangles in the last row of Fig. 8 are interchanged. Therefore, the structure was refined together with the additional positions using appropriate constraints for the occupancy and displacement parameters. The resulting occupancy parameters for the metal atoms varied between 80.5 (8) and 89 (1)%, *i.e.* between 19.5 and 11% for the admixed structure $A'B'$; $R = 0.077$ for all 2352 F values ($F_o > 2\sigma$), $R = 0.018$ for the subcell and $R = 0.181$ for the 1826 superstructure reflections ($wR_2 = 0.0303$). For the 803 superstructure reflections with $F_o > 3\sigma$, a residual of $R = 0.128$ was obtained, thus indicating that the superstructure is essentially correct.

Unfortunately, on close inspection of the precession diagrams the reciprocal lattice of the crystal used for this refinement suggested intergrowth with a second structure. This is demonstrated in Fig. 7. A hypothetical reciprocal lattice rod with the indices *h*31 of this structure is shown in Fig. 7(*d*). The corresponding observed reciprocal lattice rod for this structure (Figs. 2*d* and 7*a*), however, contains reflections with two different shapes: elongated (ellipsoidal) and less elongated (more circular). This could be rationalized in two ways. The first rationalization is demonstrated in Fig. 7(*e*). It requires the assumption that this reciprocal lattice is composed of three domains: two twin domains of structure *B* (as shown in Fig. 7*b*) in an equal ratio and a domain (Fig. 7*c*) of the hypothetical structure *A* (second

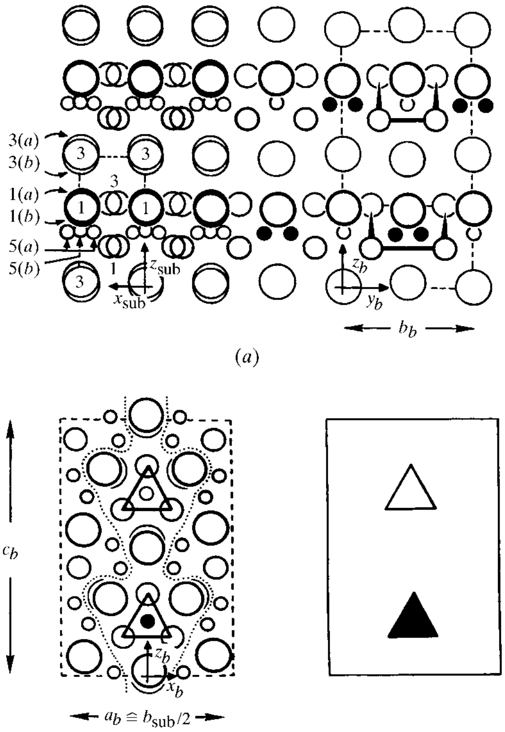

Fig. 6. The basic building block of all $Er_{10}Ru_{10}C_{19}$ superstructures. This block is shown on the right-hand side of (*a*) and in (*b*) and its dimensions a_b, b_b and c_b are indicated. On the left-hand side of (*a*) one subcell (sub) is outlined in a projection along the *y* direction. The labels 1*a*, 1*b*, 3*a*, 3*b*, 1, 3, 5*a* and 5*b* correspond to the atom designations of the Er1, Er3 (large circles), Ru1, Ru3 (medium-sized circles) and C5 (small open and filled circles) atoms of the subcell. The superstructures are caused by the ordering of the C5 atoms. Only these C5 atoms and their immediate environments (atoms encircled with dots here and in Fig. 4) are shown in part (*a*) of the figure. On the right-hand side of (*a*) and in (*b*) the ordered distribution of these atoms is shown, which leads to a doubling of the two translation periods corresponding to x_{sub} and z_{sub}. In (*c*) the ruthenium prisms surrounding the single C5*b* atoms and the $(C5a)_2$ pairs are symbolized by an open and a filled triangle, respectively. One should keep in mind that single C5*b* atoms and $(C5a)_2$ pairs also alternate in the projection direction of these building blocks.

row of Fig. 8). This model could be refined; however, the displacement parameters for many atomic positions were not well behaved. The second rationalization is demonstrated in Fig. 7(*f*). It requires the superposition (in reciprocal space; intergrowth in real space) of domains of superstructure *AB* (already solved) with domains of structure *A*. During the refinement, difference Fourier syntheses again indicated that the additional domain *A′B′* had to be considered. This model with the three domains *AB*, *A′B′* and *A* was successfully refined. The occupancy parameters for the atomic positions were constrained to be equal for all atomic positions within one domain. They were 80, 11 and 9% for the three domains with the structures *AB*, *A′B′* and *A*, respectively. Thus, in contrast to the refinement of structure *B*, we did not allow different scale factors for the subcell and superstructure reflections, which could have accounted for the diffuse scattering caused by the short-range order and the missing long-range order of superstructure *AB*. This seemed to be justified, because the superstructure reflections in the *AB* crystal were less diffuse. Also, they are much closer together than in crystal *B* (*cf.* Figs. 2*d* and 2*b*) and, therefore, a greater portion of the diffuse scattering is measured as part of the intensities of the superstructure reflections. We had tried to refine the *AB* structure with different scale factors for the subcell and superstructure reflections. However, this resulted in correlations being too strong between these scale factors, the displacement parameters and the constrained occupancy parameters (which had to account for the ratios of the three different domains). We therefore preferred to use only one scale factor for the whole data set, as is usually the case, and hence neglect the diffuse scattering.

We considered this model with the three domains *AB*, *A′B′* and *A* as the most satisfactory solution for the observed data of crystal *AB*, even though the standard deviations for the *AB* structure with this model were not smaller than those obtained in the previous refinement. It is reassuring that all positional parameters of the two refinements agreed to within three standard deviations. The final residuals for this structure are given in Table 2. The positional parameters are deposited along with the interatomic distances, which are essentially the same as the corresponding distances of the other superstructure *B*. Also deposited are the F_o/F_c tables as well as the atomic positions of structure *A*, which were used for the refinement of this data set. These positions were not allowed to vary during the refinement.†

6. Discussion

The nine carbides $Ln_{10}Ru_{10}C_{19}$ (Ln = Y, Gd–Lu) are reported here for the first time. Their Guinier powder patterns are all very similar. They could all be inter-

† See deposition footnote on p. 839.

Table 5. *Atomic parameters of superstructure B of $Er_{10}Ru_{10}C_{19}$*

All atomic positions are fully occupied. The atom designations reflect the designations as used for the refinements of the subcell data (Table 3).

	Cm	*x*	*y*	*z*	B_{eq}
Er1*aα*	2(*a*)	0.2544 (1)	0.0	0.2144 (1)	0.30 (2)
Er1*aβ*	2(*a*)	0.1416 (1)	0.0	0.7647 (1)	0.26 (2)
Er1*bα*	2(*a*)	0.7511 (1)	0.0	0.2412 (1)	0.24 (2)
Er1*bβ*	2(*a*)	0.6251 (1)	0.0	0.7373 (1)	0.25 (2)
Er2*aα*	2(*a*)	0.8217 (1)	0.0	0.6003 (2)	0.34 (2)
Er2*aβ*	2(*a*)	0.0164 (1)	0.0	0.3805 (2)	0.30 (2)
Er2*bα*	2(*a*)	0.5108 (1)	0.0	0.3639 (2)	0.30 (2)
Er2*bβ*	2(*a*)	0.3232 (1)	0.0	0.6136 (2)	0.37 (2)
Er3*a*	2(*a*)	0.4784 (1)	0.0	0.9892 (2)	0.47 (2)
Er3*b*	2(*a*)	0.9999 (1)	0.0	0.9897 (1)	0.28 (2)
Ru1*α*	4(*b*)	0.8832 (1)	0.7858 (2)	0.1356 (1)	0.27 (2)
Ru1*β*	4(*b*)	0.8102 (1)	0.2136 (2)	0.8434 (1)	0.26 (2)
Ru2*α*	4(*b*)	0.67643 (9)	0.7410 (3)	0.3960 (1)	0.33 (2)
Ru2*β*	4(*b*)	0.47301 (9)	0.7463 (4)	0.5830 (1)	0.41 (2)
Ru3	4(*b*)	0.67739 (9)	0.7834 (2)	0.9895 (1)	0.17 (2)
C1*α*	4(*b*)	0.619 (1)	0.750 (4)	0.157 (2)	0.3 (1)
C1*β*	4(*b*)	0.535 (1)	0.751 (4)	0.821 (2)	0.4 (2)
C2*α*	4(*b*)	0.539 (1)	0.740 (3)	0.196 (1)	0.2 (2)
C2*β*	4(*b*)	0.934 (1)	0.757 (4)	0.782 (2)	0.5 (2)
C3*α*	4(*b*)	0.887 (1)	0.754 (4)	0.349 (2)	0.5 (2)
C3*β*	4(*b*)	0.707 (1)	0.750 (4)	0.632 (1)	0.2 (1)
C4*α*	4(*b*)	0.325 (1)	0.763 (3)	0.424 (1)	0.1 (2)
C4*β*	4(*b*)	0.609 (1)	0.749 (4)	0.556 (1)	0.1 (1)
C5*a*	4(*b*)	0.788 (1)	0.596 (2)	0.987 (2)	0.2 (2)
C5*b*	2(*a*)	0.790 (2)	0.0	0.990 (3)	0.3 (3)

preted on the basis of the orthorhombic subcell structure, which was determined for the erbium compound. Similar superstructures as found for the erbium compound can be expected for the other 10:10:19 carbides. Even though solving the complete superstructures has taken most of the time of the present investigation, the basic structural chemistry of the 10:10:19 carbides can be discussed by considering the subcell. After all, essentially the environments of all atomic positions are similar in the subcell and the superstructures, with exceptions concerning the C5 atoms and their immediate environments.

The composition of the 10:10:19 carbides is quite similar to the composition of the $GdRuC_2$ carbide (*i.e.* 10:10:20), which is stable only in a narrow temperature range below its melting point (Hoffmann *et al.*, 1995). The structure of $GdRuC_2$ is very simple with only three atomic positions. Even though this structure is quite different from those of the 10:10:19 carbides, the near-neighbour environments are similar.

The three different Er atoms of the $Er_{10}Ru_{10}C_{19}$ subcell are all situated in trigonal prisms of Ru atoms (Fig. 5) with Er—Ru distances covering the range between 2.873 (1) and 3.281 (1) Å. The average Er—Ru distances of the Er1, Er2 and Er3 atoms are 2.942, 2.981 and 3.141 Å, respectively; the average Er3—Ru distance is greater than the others because the Er3 atom has more carbon neighbours (9.5 on average) than the other Er atoms (7.5 for Er1 and 6 for Er2). Certainly more important than the erbium–ruthenium interactions are the erbium–carbon interactions. The Er—C distances vary between 2.56 (2) and 2.83 (2) Å, and the average Er—C distances of 2.64, 2.58 and 2.65 Å somewhat reflect the number of carbon neighbours, which are (on average) 7.5, 6 and 9.5 for the Er1, Er2 and Er3 atoms, respectively. The ruthenium–carbon coordinations of these three Er atoms are augmented by 5, 5 and 6 erbium neighbours, respectively, thus increasing the total coordination numbers (CN) of the Er atoms to 18.5, 17 and 21.5 (Fig. 5). The Gd atom in $GdRuC_2$ has a CN of 18 with six ruthenium (again forming a trigonal prism), eight carbon and four gadolinium neighbours and, therefore, it is most similar in its environment to the Er1 atoms of $Er_{10}Ru_{10}C_{19}$.

The three different ruthenium positions in the subcell of $Er_{10}Ru_{10}C_{19}$ may all be considered to have trigonal prismatic erbium coordination. The Ru2 atom is situated almost in the centre of its erbium prism, while the Ru1 and Ru3 atoms are located close to one rectangular face of their respective trigonal erbium prisms. The Ru atoms are also strongly bonded to between (on average) 3.5 and 5 C atoms; most of these are situated outside the rectangular faces of the prisms formed by the Er atoms (Fig. 5). The bonding Ru—C distances vary between 2.03 (2) and 2.33 (2) Å. Exceptions are the distances of the Ru atoms to the C5 atoms of the subcell, which are not very meaningful, since the positions of the C5 atoms could not be refined well together with the anisotropic displacement parameters of the C5 atoms (upper part of Table 3). For the interatomic distances concerning the C5 atoms it is more appropriate to consult the distances of the superstructure as listed in Table 6. In addition,

Table 6. *Interatomic distances in B-$Er_{10}Ru_{10}C_{19}$*

Standard deviations are all equal to or less than 0.003 (Er—Er, Er—Ru, Ru—Ru) and 0.03 Å (Er—C, Ru—C, C—C). All distances shorter than 4.1 (Er—Er, Er—Ru, Ru—Ru), 3.9 (Er—C) and 2.9 Å (Ru—C, C—C) are listed.

Er1aα—2C1α	2.58	Er1aβ—2C5a	2.55	Er1bα—2C1α	2.55	Er1bβ—2C4β	2.51
Er1aα—2C5a	2.59	Er1aβ—2C1β	2.58	Er1bα—2C4α	2.58	Er1bβ—2C1β	2.55
Er1aα—2C4α	2.61	Er1aβ—2C3β	2.61	Er1bα—2C3α	2.59	Er1bβ—2C3β	2.59
Er1aα—2C3α	2.65	Er1aβ—2C4β	2.66	Er1bα—1C5b	2.77	Er1bβ—1C5b	2.78
Er1aα—2Ru3	2.944	Er1aβ—2Ru3	2.943	Er1bα—2Ru3	2.823	Er1bβ—2Ru3	2.827
Er1aα—2Ru2α	3.020	Er1aβ—2Ru2β	3.042	Er1bα—2Ru2α	2.882	Er1bβ—2Ru2β	2.856
Er1aα—2Ru1α	3.080	Er1aβ—2Ru1β	3.086	Er1bα—2Ru1α	2.950	Er1bβ—2Ru1β	2.950
Er1aα—1Er2bα	3.484	Er1aβ—1Er2bβ	3.493	Er1bα—1Er2aα	3.357	Er1bβ—1Er2bα	3.493
Er1aα—1Er3b	3.570	Er1aβ—1Er3b	3.567	Er1bα—1Er2aβ	3.603	Er1bβ—1Er2aα	3.599
Er1aα—2Er1bα	3.621	Er1aβ—1Er2aβ	3.605	Er1bα—2Er1aα	3.621	Er1bβ—2Er1aβ	3.621
Er1aα—1Er2bβ	3.747	Er1aβ—2Er1bβ	3.621	Er1bα—1Er3a	3.854	Er1bβ—1Er3a	3.853
Er2aα—2C3β	2.56	Er2aβ—2C3α	2.52	Er2bα—2C3α	2.54	Er2bβ—2C3β	2.53
Er2aα—2C4α	2.60	Er2aβ—2C4β	2.54	Er2bα—2C2α	2.65	Er2bβ—2C4α	2.56
Er2aα—2C2β	2.63	Er2aβ—2C2α	2.64	Er2bα—2C4β	2.65	Er2bβ—2C2β	2.63
Er2aα—2Ru2β	2.887	Er2aβ—2Ru2α	2.869	Er2bα—2Ru2α	2.977	Er2bβ—2Ru2β	2.951
Er2aα—2Ru1β	2.935	Er2aβ—2Ru2β	2.933	Er2bα—2Ru2β	3.057	Er2bβ—2Ru2α	2.992
Er2aα—2Ru2α	3.001	Er2aβ—2Ru1α	2.949	Er2bα—2Ru1α	3.137	Er2bβ—2Ru1β	3.148
Er2aα—1Er1bα	3.357	Er2aβ—1Er1bα	3.603	Er2bα—1Er1aα	3.484	Er2bβ—1Er1aβ	3.493
Er2aα—1Er1bβ	3.599	Er2aβ—1Er1aβ	3.605	Er2bα—1Er1bβ	3.493	Er2bβ—1Er3a	3.611
Er2aα—2Er2bβ	3.612	Er2aβ—2Er2bα	3.613	Er2bα—1Er3a	3.603	Er2bβ—2Er2aα	3.612
Er2aα—1Er3b	3.814	Er2aβ—1Er3b	3.828	Er2bα—2Er2aβ	3.613	Er2bβ—1Er1aα	3.747
Er3a—2C2β	2.68	Er3b—2C2α	2.60	Er3a—2Ru3	3.294	Er3b—2Ru3	3.299
Er3a—2C2α	2.69	Er3b—2C2β	2.62	Er3a—1Er2bα	3.603	Er3b—1Er1aβ	3.567
Er3a—2C1β	2.78	Er3b—2C1α	2.64	Er3a—1Er2bβ	3.611	Er3b—1Er1aα	3.570
Er3a—2C1α	2.78	Er3b—2C1β	2.64	Er3a—2Er3b	3.623	Er3b—2Er3a	3.623
Er3a—2C5a	2.86			Er3a—1Er1bβ	3.853	Er3b—1Er2aα	3.814
Er3a—2Ru1β	3.132	Er3b—2Ru1α	3.037	Er3a—1Er1bα	3.854	Er3b—1Er2aβ	3.828
Er3a—2Ru1α	3.132	Er3b—2Ru1β	3.036				
Ru1α—1C5a	2.12	Ru1β—1C5a	2.09	Ru2α—1C4α	2.08	Ru2β—1C4β	2.09
Ru1α—1C3α	2.13	Ru1β—1C3β	2.12	Ru2α—1C4β	2.17	Ru2β—1C4α	2.17
Ru1α—1C2α	2.14	Ru1β—1C2β	2.12	Ru2α—1C1α	2.23	Ru2β—1C3α	2.22
Ru1α—1C5b	2.22	Ru1β—1C5b	2.22	Ru2α—1C3β	2.24	Ru2β—1C1β	2.22
Ru1α—1Ru1β	2.722	Ru1β—1Ru1α	2.722	Ru2α—1C2α	2.25	Ru2β—1C2β	2.26
Ru1α—1Ru3	2.819	Ru1β—1Ru3	2.820	Ru2α—1Ru2α	3.480	Ru2β—1Ru2β	3.557
Ru1α—1Ru1α	3.092	Ru1β—1Ru1β	3.084	Ru2α—1Ru2α	3.740	Ru2β—1Ru2β	3.663
Ru1α—1Ru1α	4.127	Ru1β—1Ru1β	4.135	Ru2α—1Er2aβ	2.869	Ru2β—1Er1bβ	2.856
Ru1α—1Er2aβ	2.949	Ru1β—1Er2aα	2.935	Ru2α—1Er1bα	2.882	Ru2β—1Er2aα	2.887
Ru1α—1Er1bα	2.950	Ru1β—1Er1bβ	2.950	Ru2α—1Er2bα	2.977	Ru2β—1Er2aβ	2.933
Ru1α—1Er3b	3.037	Ru1β—1Er3b	3.036	Ru2α—1Er2bβ	2.992	Ru2β—1Er2bβ	2.951
Ru1α—1Er1aα	3.080	Ru1β—1Er1aβ	3.086	Ru2α—1Er2aα	3.001	Ru2β—1Er1aβ	3.042
Ru1α—1Er3a	3.132	Ru1β—1Er3a	3.132	Ru2α—1Er1aα	3.020	Ru2β—1Er2bα	3.056
Ru1α—1Er2bα	3.137	Ru1β—1Er2bβ	3.148				
Ru3—1C5a	2.11	Ru3—1Ru1α	2.819	Ru3—1Er1bα	2.823	Ru3—1Er3a	3.294
Ru3—1C1α	2.15	Ru3—1Ru1β	2.820	Ru3—1Er1bβ	2.827	Ru3—1Er3b	3.299
Ru3—1C1β	2.16	Ru3—1Ru3	3.127	Ru3—1Er1aβ	2.943		
Ru3—1C5b	2.26	Ru3—1Ru3	4.092	Ru3—1Er1aα	2.944		
C1α—1C2α	1.35	C1β—1C2β	1.37	C2α—1C1α	1.35	C2β—1C1β	1.37
C1α—1Ru3	2.15	C1β—1Ru3	2.16	C2α—1Ru1α	2.14	C2β—1Ru1β	2.12
C1α—1Ru2α	2.23	C1β—1Ru2β	2.22	C2α—1Ru2α	2.25	C2β—1Ru2β	2.26
C1α—1Er1bα	2.55	C1β—1Er1bβ	2.55	C2α—1Er3b	2.60	C2β—1Er3b	2.63
C1α—1Er1aα	2.58	C1β—1Er1aβ	2.58	C2α—1Er2aβ	2.64	C2β—1Er2bβ	2.63
C1α—1Er3b	2.64	C1β—1Er3b	2.64	C2α—1Er2bα	2.65	C2β—1Er2aα	2.63
C1α—1Er3a	2.78	C1β—1Er3a	2.78	C2α—1Er3a	2.69	C2β—1Er3a	2.68
C3α—1C4α	1.38	C3β—1C4β	1.35	C4α—1C3α	1.38	C4β—1C3β	1.35
C3α—1Ru1α	2.13	C3β—1Ru1β	2.12	C4α—1Ru2α	2.08	C4β—1Ru2β	2.09
C3α—1Ru2β	2.22	C3β—1Ru2α	2.24	C4α—1Ru2β	2.17	C4β—1Ru2α	2.17
C3α—1Er2aβ	2.52	C3β—1Er2bβ	2.53	C4α—1Er2bβ	2.56	C4β—1Er1bβ	2.51
C3α—1Er2bα	2.54	C3β—1Er2aα	2.56	C4α—1Er1bα	2.58	C4β—1Er2aβ	2.54

Table 6 (*cont.*)

C3α−1Er1*b*α	2.59	C3β−1Er1*b*β	2.59	C4α−1Er2*a*α	2.60	C4β−1Er2*b*α	2.65
C3α−1Er1*a*α	2.65	C3β−1Er1*a*β	2.61	C4α−1Er1*a*α	2.61	C4β−1Er1*a*β	2.66
C5*a*−1C5*a*	1.39			C5*b*−2Ru1α	2.22	C5*b*−1Er1*b*α	2.77
C5*a*−1Ru1β	2.09	C5*a*−1Er1*a*β	2.55	C5*b*−2Ru1β	2.22	C5*b*−1Er1*b*β	2.78
C5*a*−1Ru3	2.11	C5*a*−1Er1*a*α	2.59	C5*b*−2Ru3	2.26		
C5*a*−1Ru1α	2.12	C5*a*−1Er3*a*	2.86				

there are Ru−Ru bonds. The Ru1 atom has one ruthenium neighbour at 2.720 (1) Å and another one at 2.819 (1) Å; the Ru3 atom has two, both at 2.819 (1) Å. The Ru−Ru distances of 3.61 Å are too long to be counted as bonding distances. In $GdRuC_2$ the Ru atoms are situated in an octahedron of Gd atoms with (in addition) four carbon neighbours at 2.14 Å and two ruthenium neighbours at 2.60 Å each.

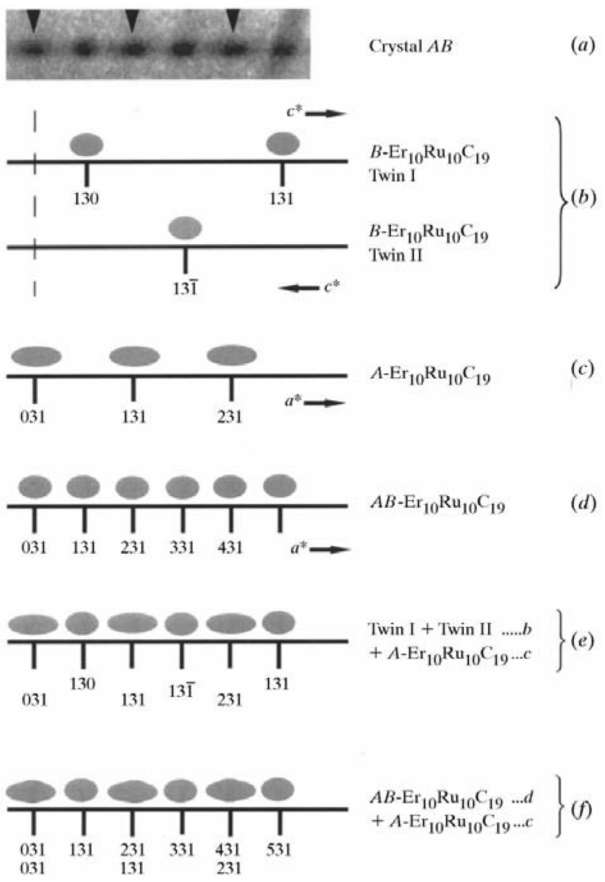

Fig. 7. Analysis of the reciprocal lattice reflections of crystal *AB*. The reciprocal lattice of this crystal has orthorhombic symmetry and the shown reciprocal lattice row is reproduced from a first upper-level precession photograph. The first row (*a*) displays an enlargement of those superstructure reflections of crystal *AB* which are enframed in Fig. 2(*d*). A naive assignment of indices to this orthorhombic lattice results in the indices as shown in row (*d*). However, the reciprocal lattice row (*a*) contains alternating (nearly) circular and ellipsoidal reflections and this can be interpreted in various ways, as is further discussed in the text.

The C1 and C2 atoms as well as C3 and C4 in the subcell of $Er_{10}Ru_{10}C_{19}$ form pairs with C−C bond distances of 1.36 (4) and 1.38 (4) Å, respectively, slightly longer than the C=C double-bond distance of 1.35 Å in olefins. These C_2 pairs are situated in trigonal prisms of Er atoms. The rectangular faces of these erbium prisms are capped by Ru atoms, thus increasing the CN of these carbon pairs to nine. The environments of these pairs do not change in going from the subcell to the various superstructures.

The positions of the C5 atoms provide the key to understanding the superstructures. They are located in trigonal prisms formed by six Ru atoms, with three additional Er atoms outside the rectangular faces of the ruthenium prisms. In the subcell refinement with unsplit atomic positions (upper part of Table 3) the C5 atoms occupy 75% of a 4(*c*) position with the (impossibly short) C5−C5 bond distance 0.80 (1) Å. In the refinement with split atomic positions (lower part of Table 3) the C5 atoms are located on two atomic sites [4(*c*) and 2(*a*)], each with 50% occupancies. The C5*a* atoms form pairs within an elongated prism of Ru atoms, now with a bond distance of 1.52 (6) Å [refinement of the superstructures reveals that the real C−C distance of the C5*a* pairs is 1.39 (3) Å], while the C5*b* atoms are single atoms, occupying the centre of a compressed trigonal prism formed by the Ru atoms. The various superstructures of $Er_{10}Ru_{10}C_{19}$ arise from the ordered arrangement of the $(C5a)_2$ pairs and the single C5*b* atoms and the fact that their atomic environments reflect this order.

Of course, experimentally the superstructures are determined by the arrangement of occupied and non-occupied split positions of the metal atoms. Hence, the occupancy parameter of 0.75 for the C5 position in the refinement of the subcell with anisotropic displacement parameters (upper part of Table 3), as well as the atomic ratio 2:1 of the C5*a*-to-C5*b* positions in the refinement of the subcell with split atomic positions (lower part of Table 3), is a space requirement. The interatomic distances within the dotted lines of the building block shown in Fig. 6(*b*) are chemically reasonable only if single C5*b* and paired C5*a* atoms alternate, *i.e.* the order is perfect in two dimensions [the *xz* plane of the subcell as shown in Fig. 6(*a*), which corresponds to the *xy* plane of structure *B* and to the *yz* plane of structure *AB*]. The disorder occurs only in the third dimension. We have used the letters *A* and *B* to designate the two possibilities for the arrangement of three adjacent building blocks (Fig. 8). This is similar to the situation of cubic and hexagonal close-packed spheres, where the letters *h* and *c* are used in the Jagodzinski–Wyckoff notation (Jagodzinski, 1954*a*,*b*). In using this notation, our structures *A* and *B* correspond to the stacking sequences of hexagonal and cubic close packing, while the four-layer structure *AB* corresponds to the four-layer close-packed structure of neodymium with the Jagodzinski–Wyckoff notation $(hc)_2$.

If the number of stacked layers is limited to four within one translation period, there are only these three different structures possible – *A*, *B* and *AB*. However, if infinitely long translation periods are allowed, an infinite

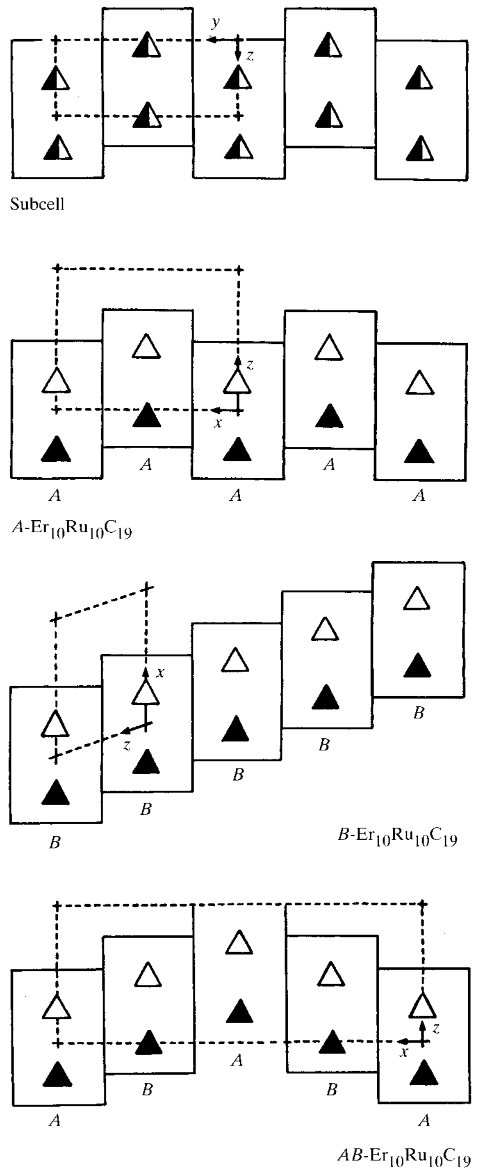

Fig. 8. The arrangement of the building blocks of Fig. 6 in the subcell and in various superstructures of $Er_{10}Ru_{10}C_{19}$. The corresponding unit cells are indicated by dashed lines. In the subcell the C5 atoms are disordered and this is symbolized by half-filled triangles. The labels *A* and *B* are used to designate the various stacking sequences of the basic building block. Note that building block *A* contains a vertical mirror plane. Thus, of the two mirror planes of the subcell (one parallel to the paper plane and the other perpendicular to the stacking direction) all are retained in *A*-$Er_{10}Ru_{10}C_{19}$, which has the stacking sequence *AA*, *AA*. In the structure of *B*-$Er_{10}Ru_{10}C_{19}$ (stacking sequence *B*, *B*) all mirror planes perpendicular to the stacking direction are lost; in *AB*-$Er_{10}Ru_{10}C_{19}$ (stacking sequence *ABAB*, *ABAB*) every other one of these is missing.

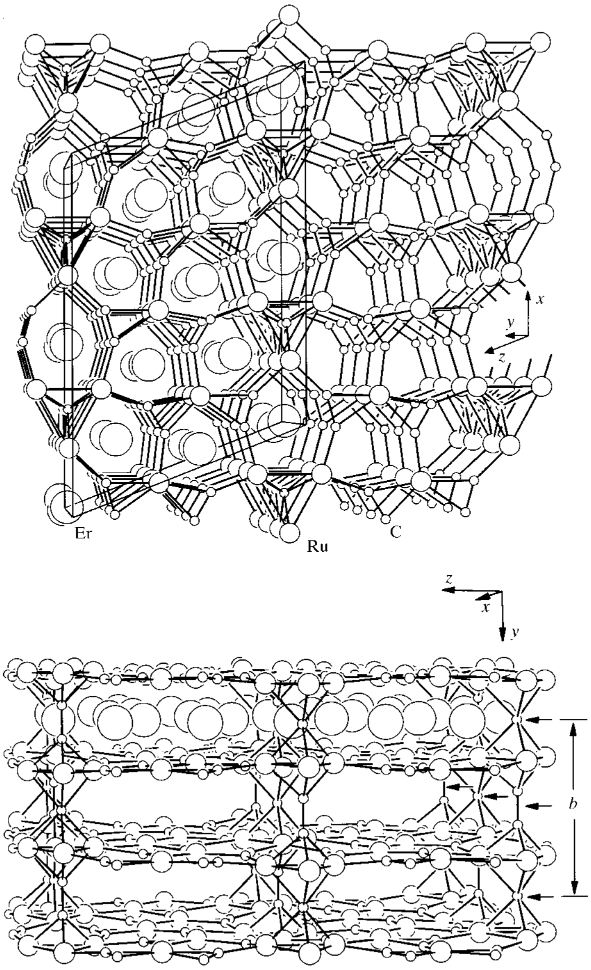

Fig. 9. The crystal structure of *B*-$Er_{10}Ru_{10}C_{19}$ shown in two projections. In both not all Er atoms are drawn, to aid visualization of the ruthenium–carbon polyanion. This polyanion consists of two-dimensionally infinite nets, which are viewed from above in the upper part of the figure and from the side in the lower part. These nets are connected by carbon pairs and single C atoms (arrows), which alternate along the *y* direction, and this is the reason for the doubled *b* axis of this and all other superstructures. Single C atoms and C_2 pairs between the Ru atoms of the adjacent nets also alternate along the *x* direction and this leads to the doubled *a* translation period of superstructure *B*. In the other superstructures the corresponding translation periods are also doubled. The differences between the various superstructures result from the length and the orientation of the third translation period (Fig. 8).

number of possibilities exist for the stacking of these layers. We have refined two of them (structures *B* and *AB*). In addition, we have found evidence for substantial disorder, especially for the subcell crystal, where no well resolved superstructure reflections were observed. The disorder in this crystal may be determined by analysing the diffuse diffraction streaks according to the theory developed for OD (order–disorder) structures (Jagodzinski, 1949*a*,*b*; Gevers, 1954; Dornberger-Schiff, 1956; Kakinoki & Komura, 1965; Takaki, 1977; Müller, 1979), which has been used for many disordered structures (Jagodzinski, 1949*c*; Schwarzenbach, 1969; Takaki *et al.*, 1975; Blanc *et al.*, 1996).

The Ru and C1, C2, C3 and C4 atoms form a slightly puckered, two-dimensionally infinite, polyanionic net, which is emphasized in the upper part of Fig. 4. Such nets are stacked on top of each other, as shown in Fig. 9. Viewed from the side (lower part of Fig. 9), it can be seen that the two-dimensionally infinite polyanionic layers are interconnected by alternating carbon pairs and single C atoms. These are the C5 atoms. The whole structure may also be imagined as a 'multiple floor garage', where the ruthenium–carbon nets correspond to the floors, the C5 atoms to the pillars and the Er atoms to the cars. Thus, the structure has some similarity to that of the well known solid electrolyte β-alumina ($\sim NaAl_{11}O_{17}$), where the Na atoms are highly mobile. A similar mobility cannot be expected for the Er atoms, since they carry a higher charge and, therefore, they are more tightly bonded to their local ruthenium–carbon environments.

Chemical bonding in the various structures of $Er_{10}Ru_{10}C_{19}$ can, to a first approximation, be rationalized by simple concepts. For this rationalization we neglect any bonding Er–Er interactions, an assumption which is an oversimplification considering that the shortest Er–Er distance is 3.36 Å (Table 6: Er1*bα*—Er2*aα*), compared with the average Er—Er distance of 3.51 Å in the hexagonal close-packed structure of elemental erbium (Donohue, 1974). Nevertheless, the Er atoms, as the most electropositive components of the compound, may be assumed to have largely transferred their valence electrons to the ruthenium–carbon polyanion. For simplicity, we also assume the C atoms of the

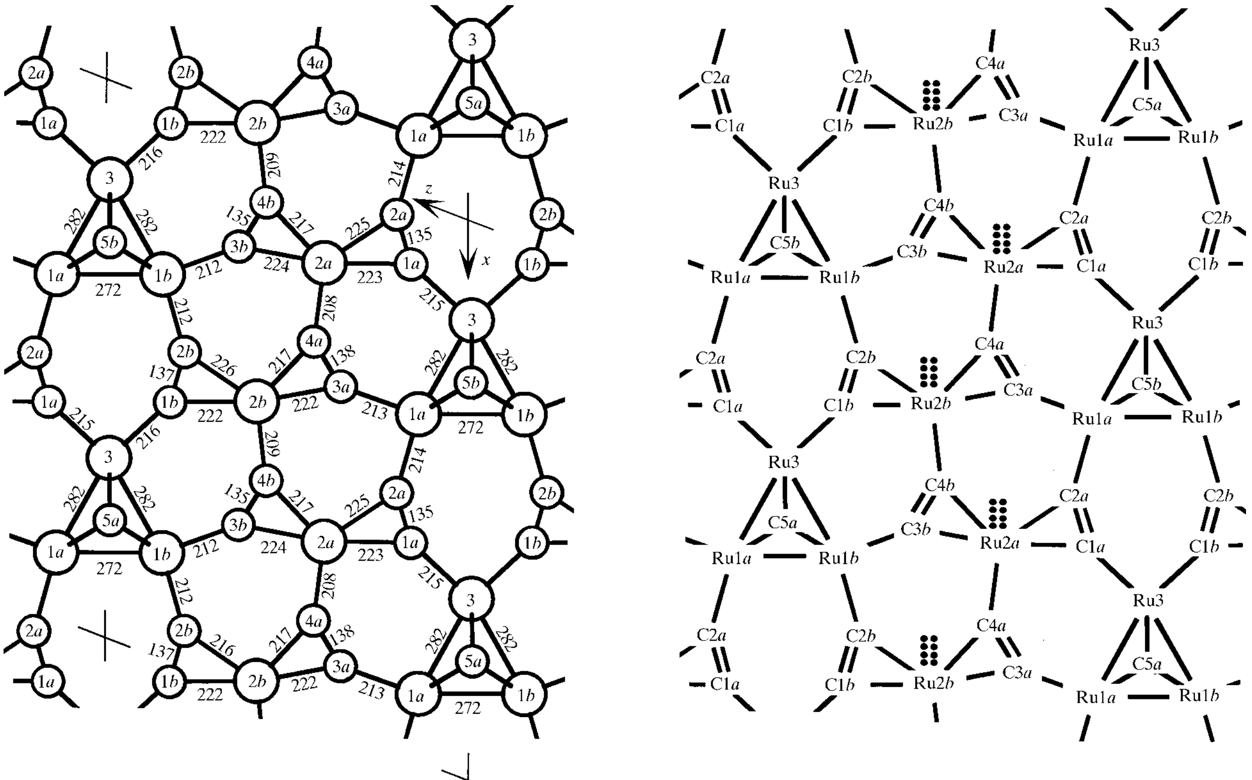

Fig. 10. Polyanion of *B*-$Er_{10}Ru_{10}C_{19}$. On the left-hand side the interatomic distances (pm) within the two-dimensionally infinite polyanion are shown. Large and small circles represent Ru and C atoms, respectively. The numbers and letters within the circles correspond to the atom designations. C5*a* and C5*b* are above and below the plane of the flat polyanion, thus connecting the polyanions in the third dimension. On the right-hand side, a valence electron distribution is shown, assuming two-electron bonds for each Ru—C interaction and that the octet and 18-electron rules are obeyed by the C and Ru atoms, respectively. The full electron count is shown only for the Ru2 atoms; see the caption to Fig. 11 regarding Ru1, Ru3 and C5.

C_2 pairs to form double bonds, *i.e.* they derive from ethylene, C_2H_4. In counting the electrons of the ruthenium–carbon bonds at the C atoms and assuming the octet rule for the C atoms to be obeyed, each C_2 pair obtains a formal charge of 4−. Similarly, the isolated C5*b* atoms located inside the trigonal prisms of the Ru atoms also obtain a formal charge of 4−. The compound can then be written with the formula $[10Er^{3+}]^{30+}[Ru_{10}C_{19}]^{30-}$, where the ruthenium–carbon polyanion is emphasized; or we can express this in more detail with the formula $[10Er^{3+}]^{30+}[(4Ru1.2Ru3).(4Ru2)]^{10+}[8(C_2^{4-}).(C5a_2^{4-}).(C5b^{4-})]^{40-}$, where the superscripts represent oxidation numbers (formal charges). The important result of this account is that the ten Ru atoms together carry a formal charge of 10+, *i.e.* the average Ru atom has a d^7 system.

We have frequently observed in similar carbides that the transition metal atoms have an environment which is compatible with the 18-electron rule, *e.g.* in Pr_2ReC_2 (Jeitschko *et al.*, 1990), $Ca_4Ni_3C_5$ (Musanke & Jeitschko, 1991), $Th_4Ni_3C_6$ (Moss & Jeitschko, 1991), $Sc_5Re_2C_7$ (Pöttgen & Jeitschko, 1992), $Gd_3Mn_2C_6$ (Kahnert & Jeitschko, 1993), $Yb_4Ni_2C_5$ (Musanke, Jeitschko & Danebrock, 1993), $La_{12}Re_5C_{15}$ (Pöttgen *et al.*, 1994) and $GdRuC_2$ (Hoffmann *et al.*, 1995). This is also the case for the Ru atoms in the various superstructures of $Er_{10}Ru_{10}C_{19}$. For this account we start with the Ru2 atoms. They are located in a two-dimensionally infinite part of the ruthenium–carbon polyanion (corresponding to the stacked floors in a parking garage, as outlined in the lower part of Fig. 9). This two-dimensionally infinite net is shown in Fig. 10. It can be seen that all Ru2 atoms are coordinated by two pairs of C atoms 'side-on' and by another pair of C atoms 'end-on'. On the right-hand side of Fig. 10 a possible valence electron distribution for the two-dimensionally infinite net is shown using the Lewis formalism and assuming two-electron bonds for each Ru—C contact. If the 18-electron rule is to be obeyed by the Ru2 atoms, each ought to have eight non-bonding electrons (*i.e.* a 'd^8 system'). We thus arrive at the more detailed chemical formula $[10Er^{3+}]^{30+}[(4Ru1.2Ru3)^{10+}(4Ru2)^{0\pm}]^{10+}[8(C_2^{4-}).(C5a_2^{4-}).(C5b^{4-})]^{40-}$, where the four Ru1 and the two Ru3 atoms together carry a formal charge of 10+.

The two-dimensionally infinite layers of the Ru and C atoms shown in Fig. 10 are connected in the third

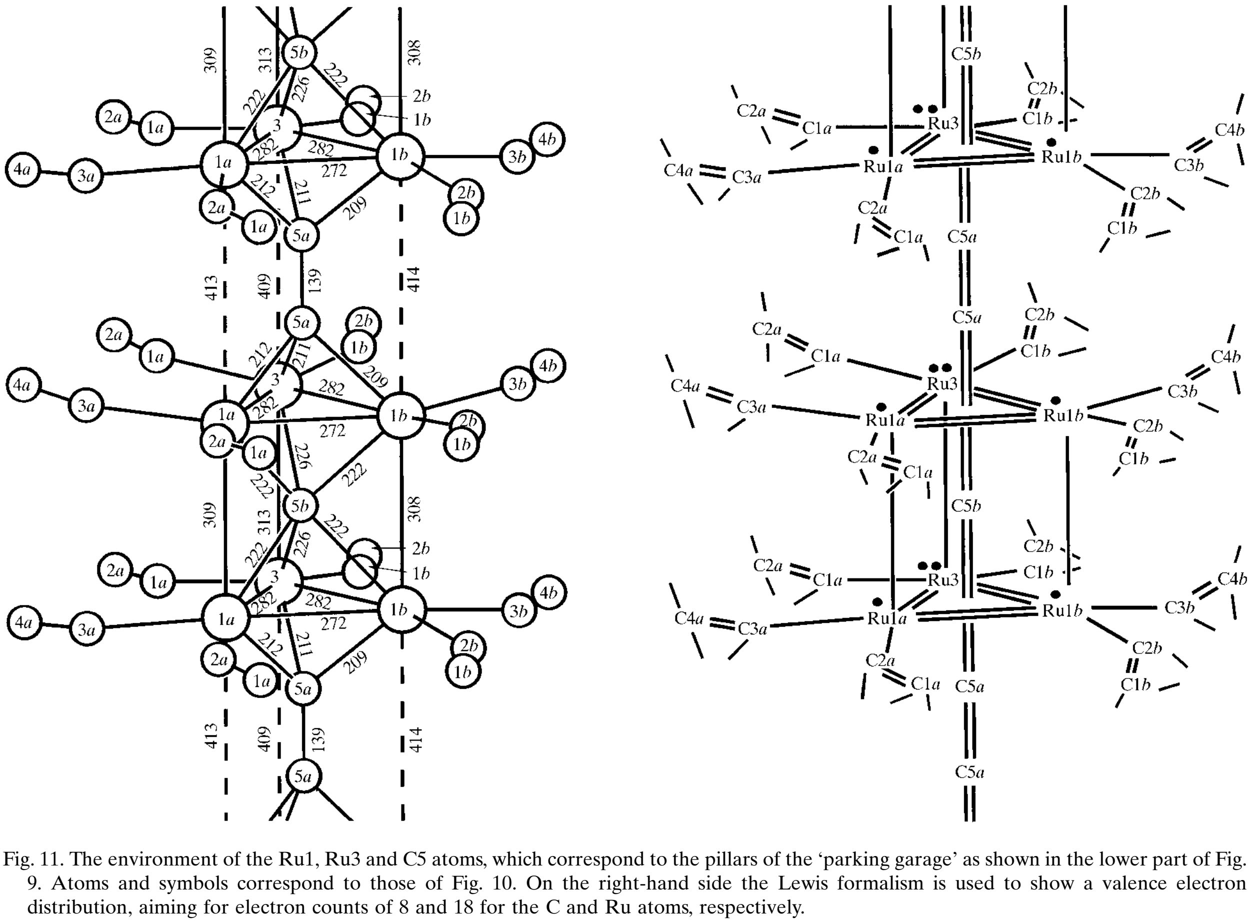

Fig. 11. The environment of the Ru1, Ru3 and C5 atoms, which correspond to the pillars of the 'parking garage' as shown in the lower part of Fig. 9. Atoms and symbols correspond to those of Fig. 10. On the right-hand side the Lewis formalism is used to show a valence electron distribution, aiming for electron counts of 8 and 18 for the C and Ru atoms, respectively.

dimension *via* the C5 atoms. The arrangement of these atoms together with the adjacent Ru1 and Ru3 atoms is shown in Fig. 11. Four Ru1 and two Ru3 atoms form a trigonal prismatic Ru_6 cluster. It can be seen that the Ru atoms of these clusters all have similar chemical environments. Each Ru atom is coordinated by two C_2 pairs end-on, which are located in a horizontal plane also containing the triangular faces of the trigonal prisms of the Ru_6 clusters. The C5*b* atoms are located within the Ru_6 clusters, while the C5*a* atoms are situated outside the clusters. They form pairs which connect two adjacent Ru_6 prisms *via* their triangular faces. On the right-hand side of Fig. 11 a possible valence electron distribution is shown, again using the Lewis formalism and aiming for 18 electrons for each Ru atom. In the electron distribution shown in Fig. 11 each Ru atom 'sees' four electrons belonging to the two C_2 pairs within the horizontal plane, $2 \times \frac{4}{3}$ of an electron from the C5 atoms and 10 electrons from the Ru—Ru bonds within the Ru_6 cluster. This amounts to a total of 16.66 electrons per Ru atom. In addition, we see eight non-bonding electrons per Ru_6 cluster, which we have arbitrarily distributed between the Ru1 and Ru3 atoms in order to avoid drawing fractional electrons. Hence, on average each Ru atom also has $\frac{8}{6} = \frac{4}{3}$ non-bonding electrons and, together with the 16.66 bonding electrons enumerated above, each Ru atom obtains 18 electrons. In order to achieve this satisfying result we had to assume double bonds within the Ru_3 triangles and single bonds for the Ru—Ru interactions between the Ru_3 triangles of a Ru_6 cluster. This correlates with the Ru—Ru bond lengths, as can be seen from the left-hand side of Fig. 11: the Ru—Ru double bonds correspond to bond lengths of 2.72 and 2.82 Å, while single bonds were assigned to the Ru—Ru interactions with bond lengths of 3.08, 3.09 and 3.13 Å. Hence, the total number of electrons, using only ruthenium orbitals, is 38 per Ru_6 cluster: eight non-bonding electrons plus 30 electrons forming Ru–Ru bonds, *i.e.* on average, each of the six Ru1 and Ru3 atoms obtains a $d^{6.33}$ system, in agreement with their formal charge of 10+ in the formula derived in the preceding paragraph.

The total number of electrons per Ru_6 cluster (including the electrons involved in Ru—C bonding) is now also easily established. Since each Ru atom has 18 electrons, we count $6 \times 18 = 108$ electrons; from these we have to subtract one half of the thirty, which are involved in Ru—Ru bonding, since these were counted twice. We therefore arrive at an electron count of $108 - 30/2 = 93$ per Ru_6 cluster. This number is already close to the ideal electron count of 90 found for trigonal prismatic transition metal clusters in molecular compounds (Tachikawa & Muetterties, 1981; Wijeyesekera & Hoffmann, 1984; Mingos & May, 1990). However, if we allow for some Er—Er bonding (thereby lowering the formal charge of the ruthenium–carbon polyanion), as mentioned in the beginning of this discussion, we may well arrive at the same electron count for the trigonal prismatic Ru_6 clusters in this solid, as was established for such clusters in molecules.

We thank Dipl.-Ing. U. Ch. Rodewald and Dr M. H. Möller for the competent collection of the single-crystal diffractometer data, Dr C. B. H. Evers for the electrical conductivity measurements, Dr K. Zeppenfeld for the determination of the magnetic properties, Mr K. Wagner for the work at the scanning electron microscope and Mrs U. Göcke for her help with the drawings. We also acknowledge Dr W. Gerhartz (Degussa AG) and Dr G. Höfer (Heraeus Quarzschmelze) for generous gifts of ruthenium powder and silica tubes, respectively. This work was supported by the Deutsche Forschungsgemeinschaft and the Fond der Chemischen Industrie.

References

Blanc, E., Bürgi, H.-B., Restori, R., Schwarzenbach, D. & Ochsenbein, Ph. (1996). *Europhys. Lett.* **33**, 205–210.

Donohue, J. (1974). *The Structures of the Elements*. New York: Wiley.

Dornberger-Schiff, K. (1956). *Acta Cryst.* **9**, 593–601.

Flack, H. D. (1983). *Acta Cryst.* A**39**, 876–881.

Flack, H. D. & Schwarzenbach, D. (1988). *Acta Cryst.* A**44**, 499–506.

Gevers, R. (1954). *Acta Cryst.* **7**, 492–494.

Hoffmann, R.-D. (1996). *Rwert. Program for the Calculation of R Values for Specific Classes of Reflections*. University of Münster, Germany.

Hoffmann, R.-D. & Jeitschko, W. (1987). *Z. Kristallogr.* **178**, 110.

Hoffmann, R.-D. & Jeitschko, W. (1990). *Acta Cryst.* A**46**, C-285.

Hoffmann, R.-D., Jeitschko, W. & Boonk, L. (1989). *Chem. Mater.* **1**, 580–586.

Hoffmann, R.-D., Pöttgen, R. & Jeitschko, W. (1992). *J. Solid State Chem.* **99**, 134–139.

Hoffmann, R.-D., Wachtmann, K. H., Ebel, T. & Jeitschko, W. (1995). *J. Solid State Chem.* **118**, 158–162.

Holleck, H. (1972). *J. Nucl. Mater.* **42**, 278–284.

Holleck, H. (1977). *J. Less-Common Met.* **52**, 167–172.

Jagodzinski, H. (1949*a*). *Acta Cryst.* **2**, 201–207.

Jagodzinski, H. (1949*b*). *Acta Cryst.* **2**, 208–214.

Jagodzinski, H. (1949*c*). *Acta Cryst.* **2**, 298–304.

Jagodzinski, H. (1954*a*). *Acta Cryst.* **7**, 17–25.

Jagodzinski, H. (1954*b*). *Neues Jahrb. Mineral.* **10**, 49–65.

Jeitschko, W., Block, G., Kahnert, G. E. & Behrens, R. K. (1990). *J. Solid State Chem.* **89**, 191–201.

Jeitschko, W., Gerss, M. H., Hoffmann, R.-D. & Lee, S. (1989). *J. Less-Common Met.* **156**, 397–412.

Kahnert, G. E. & Jeitschko, W. (1993). *Z. Anorg. Allg. Chem.* **619**, 93–97.

Kakinoki, J. & Komura, Y. (1965). *Acta Cryst.* **19**, 137–147.

Mingos, D. M. P. & May, A. S. (1990). *The Chemistry of Metal Cluster Complexes*, edited by D. F. Shriver, H. D. Kaesz & R. D. Adams, pp. 11–120. Weinheim: VCH Verlagsgesellschaft.

Moss, M. A. & Jeitschko, W. (1991). *Z. Metallkd.* **82**, 669–674.

Müller, U. (1979). *Acta Cryst.* A**35**, 957–961.
Musanke, U. E. & Jeitschko W. (1991). *Z. Naturforsch. Teil B*, **46**, 1177–1182.
Musanke, U. E., Jeitschko, W. & Danebrock, M. E. (1993). *Z. Anorg. Allg. Chem.* **619**, 321–326.
Musanke, U. E., Jeitschko, W. & Hoffmann, R.-D. (1993). *Z. Kristallogr.* **205**, 201–214.
Pöttgen, R., Block, G., Jeitschko, W. & Behrens, R. K. (1994). *Z. Naturforsch. Teil B*, **49**, 1081–1088.
Pöttgen, R. & Jeitschko, W. (1992). *Z. Naturforsch. Teil B*, **47**, 358–364.
Schwarzenbach, D. (1969). *Z. Kristallogr.* **128**, 97–114.
Sheldrick, G. M. (1993). *SHELXL*93. *Program for the Refinement of Crystal Structures*. University of Göttingen, Germany.
Tachikawa, M. & Muetterties, E. L. (1981). *Prog. Inorg. Chem.* **28**, 203–238.
Takaki, Y. (1977). *Acta Cryst.* A**33**, 690–693.
Takaki, Y., Kato, Y. & Sakurai, K. (1975). *Acta Cryst.* B**31**, 2753–2758.
Wachtmann, K. H., Moss, M. A., Hoffmann, R.-D. & Jeitschko, W. (1995). *J. Alloys Compd.* **219**, 279–284.
Wijeyesekera, S. D. & Hoffmann, R. (1984). *Organometallics*, **3**, 949–961.
Witte, A. M. & Jeitschko, W. (1994). *J. Solid State Chem.* **112**, 232–236.
Wondratschek, H. & Jeitschko, W. (1976). *Acta Cryst.* A**32**, 664–666.
Yvon, K., Jeitschko, W. & Parthé, E. (1977). *J. Appl. Cryst.* **10**, 73–74.